

See discussions, stats, and author profiles for this publication at: <https://www.researchgate.net/publication/332970521>

Adaptive Image Enhancement Method for Correcting Low-Illumination Images

Article in *Information Sciences* · May 2019

DOI: 10.1016/j.ins.2019.05.015

CITATIONS

79

READS

1,722

4 authors, including:



Wencheng Wang

Weifang University

37 PUBLICATIONS 943 CITATIONS

[SEE PROFILE](#)



Xiaojin Wu

23 PUBLICATIONS 535 CITATIONS

[SEE PROFILE](#)

Dear author,

Please note that changes made in the online proofing system will be added to the article before publication but are not reflected in this PDF.

We also ask that this file not be used for submitting corrections.



Contents lists available at ScienceDirect

Information Sciences

journal homepage: www.elsevier.com/locate/ins

Adaptive image enhancement method for correcting low-illumination images

q1 Wencheng Wang^{a,*}, Zhenxue Chen^b, Xiaohui Yuan^c, Xiaojin Wu^a^a College of Information and Control Engineering, Weifang University, No. 5147 Dongfeng Street, Weifang, Shandong 261061, China^b College of Control Science and Engineering, Shandong University, Jinan 250061, China^c Department of Computer Science and Engineering, University of North Texas, Denton, USA**ARTICLE INFO****Article history:**

Received 10 November 2018

Revised 4 May 2019

Accepted 8 May 2019

Available online xxx

Keywords:

Multiscale

Uneven illumination

Low illumination image

Illumination-reflection model

ABSTRACT

In this study, to improve the adaptability of image enhancement in images with low illumination, a colored image correction method based on nonlinear functional transformation according to the illumination-reflection model and multiscale theory is proposed. First, the original RGB image is converted to HSV color space, and the V component is used to extract the illumination component of the scene using the multiscale Gaussian function. Then, a correction function is constructed based on the Weber-Fechner law, and two images are obtained through adaptive adjustments to the image enhancement function parameters based on the distribution profiles of the illumination components. Finally, an image fusion strategy is formulated and used to extract the details from the two images. Compared with the classic algorithm, the proposed algorithm can improve the overall brightness and contrast of an image while reducing the impact of uneven illumination. The enhanced images appear clear, bright, and natural.

© 2019 Elsevier Inc. All rights reserved.

1. Introduction

Digital image processing systems are widely used in many areas, such as industrial production, video surveillance, intelligent transportation, and remote sensing and monitoring [40]. Thus, these systems play an important role in many fields. However, the images acquired by image acquisition systems are often flawed due to various defects that arise from a variety of uncontrollable factors during the image acquisition process, especially under unfavorable conditions such as indoor lighting, nighttime lighting, and cloudy weather [7]. Under these unfavorable conditions, the reflection of the target surface is weak, and the color is distorted by the presence of considerable noise, thus resulting in serious degradation in image quality, which prevents visual systems from fully fulfilling their purposes [4,6,12,13,42]. Therefore, obtaining clear still or moving images under low-illumination conditions has become an urgent problem to solve. Image enhancement techniques offer one possible solution, as image enhancement not only satisfies the need for a better visual experience but also improves the reliability and robustness of outdoor vision systems, which makes it easier for image processing systems to analyze and process images. Moreover, the development of image enhancement techniques boosts the development of image information mining theory [41,44,45].

As a classic issue in the field of digital image processing, low-illumination image enhancement has long been studied with constant enthusiasm, and these research methods have also been applied in different fields. For example, Du et al.

q2 * Corresponding author.

E-mail addresses: wwcwf@126.com (W. Wang), chenzhenxue@sdu.edu.cn (Z. Chen), xiaohui.yuan@unt.edu (X. Yuan), wfwuj@163.com (X. Wu).

[9] presented a novel adaptive region-based image preprocessing scheme for face recognition tasks, in which contrast enhancement and edge enhancement (EdgeE) were combined to improve the recognition accuracy. This method was suitable for addressing uneven illumination conditions in images of faces. In ref. [24], a novel enhancement algorithm was proposed for medical images. First, contrast-limited adaptive histogram equalization (CLAHE) was adopted to improve the global contrast; then, the low-frequency component and several high-frequency components were used to enhance the edge detail. The experimental results indicated the superiority of the proposed method in terms of the visual effect. Shi et al. [35] proposed a low-illumination image enhancement method for single nighttime images, which utilized the bright channel prior to obtain an initial transmission value and then used the dark channel as a complementary channel to correct the potentially erroneous transmission estimates attained from the bright channel prior. Lu et al. [28] proposed a method to address the problem of descattering in underwater images influenced by low-light conditions by using deep convolutional neural networks (CNNs) with depth estimation. Furthermore, a spectral characteristic-based color correction method was used to recover the color reduction. Alismail et al. [1] presented an algorithm for robust and real-time visual tracking under challenging illumination conditions characterized by poor lighting and sudden and drastic changes in illumination. The proposed adaptation preserved the Hamming distance under least-squares minimization, thus preserving the photometric invariance properties of binary descriptors. To address the issue of video surveillance in low-illumination conditions, Zhi et al. [50] proposed a new nonuniform image enhancement algorithm based on illumination adjustment combined with guided filtering and the "S Curve" function, which was used in a coal mine environment. Thus, image enhancement is a common problem in various fields, and how to adaptively enhance images with low illumination or uneven illumination requires further study. To address these problems, this paper proposes an adaptive low-illumination image enhancement method based on multiscale fusion. While preserving the details of the image, the proposed method balances the color across the image and discovers details that were previously invisible in dark areas, which significantly improves the image quality. This study may lend new ideas to future studies on the correction of images with uneven illumination.

The remainder of this paper is organized as follows. The second section briefly introduces the work related to low-illumination images. The third section describes the key steps of the method proposed in this paper, including space conversion, estimation of reflection components, adaptive brightness enhancement and image fusion principles. In Section 4, the experimental results are analyzed, and the conclusion is presented in Section 5.

2. Related work

Traditional low-illumination image enhancement algorithms include the gray transformation method and histogram equalization method [15]. Huang et al. [14] proposed an adaptive gamma correction algorithm to adaptively obtain gamma correction parameters based on a cumulative distribution probability histogram. Yu et al. [48] mapped the hue of an image to an appropriate range using the inverse tangent hyperbolic curve and proposed a low-illumination image enhancement method based on the optimal hyperbolic tangent profile [26]. Kim et al. [19] proposed standard adaptive histogram equalization (AHE). Kim et al. [18] employed the block iterative histogram method to enhance the contrast of an image while using a moving template to perform partially overlapped subblock histogram equalization (POSHE) on various parts of the image. Kim proposed brightness-preserving bihistogram equalization (BBHE) [23] to perform histogram equalization on two subimages resulting from threshold division; this method solved the problem of abnormal brightness variations within small areas. Later, Wang et al. proposed equal-size dualistic subimage histogram equalization (DSIHE) [46], which divides an original image into two parts of equal size to maximize the entropy of the image, thus solving the problem of image information loss that plagues the standard histogram equalization algorithm. Chen et al. proposed the minimum mean brightness error BHE (MMBEBHE) [5] algorithm to minimize the discrepancy between the mean brightness of an output image and that of the original image. Shen et al. used an iterative method to determine the segmentation threshold and proposed the iterative brightness bihistogram equalization (IBBHE) [33] method, which avoids the mistake that is often made by traditional histogram equalization techniques of confusing the target and background. Celik and Tjahjadi [3] proposed the contextual and variational contrast (CVC) enhancement algorithm, which uses the two-dimensional histogram of the input image and the context information model to perform nonlinear data mapping and thus achieves low-illumination image enhancement. These algorithms have simple mechanisms and require a low level of computational complexity; however, they are prone to image color loss and excessive noise.

Jobson et al. proposed the single-scale retinex (SSR) algorithm [16] based on the retinex illumination-reflection model established by Land et al. [21], which later evolved into the multiscale retinex (MSR) algorithm, the MSR algorithm with color restoration (MSRCR) [17,32], and the MSR algorithm with chromaticity preservation (MSRCP) [31]. Fu et al. proposed a weighted variational model for simultaneous reflection and illumination estimation (SRIE) that could preserve the estimated reflectivity with high accuracy and suppress noise to a certain extent [10]. Wang et al. [39] proposed a bright-pass filter that considered the brightness of adjacent areas to preserve the naturalness of an image. This technique, also known as naturalness-preserved enhancement (NPE), not only enhances image contrast but also prevents local overenhancement. In 2011, Dong et al. [8] proposed a method that reversed a low-illumination image to obtain an image that was similar to a photo taken on a foggy day before improving the image quality using the defogging algorithm. Subsequently, Zhang et al. combined the defogging technique and the bilateral filtering technique to produce a low-illumination image enhancement method that could process images in real time. By using the dark channel prior to estimate the parameters, the algorithm optimized the image through joint bilateral filtering, thus mitigating the influence of noise [49]. Tao et al. combined the

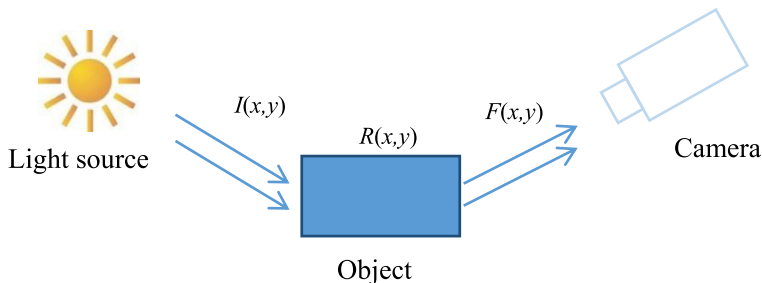


Fig. 1. Illumination-reflection model.

bright channel prior with a CNN [37], and Park et al. combined the bright channel prior with the retinex enhancement algorithm; both methods achieved good results [29].

Image enhancement methods based on machine learning have emerged in recent years [11]. Lore et al. [27] used a stacked sparse denoising autoencoder in a low-illumination image enhancement framework to develop an image enhancement technique that simulated a low-illumination environment via nonlinear darkening, the addition of Gaussian noise and a self-encoder method based on deep learning to achieve adaptive brightness adjustment and denoising through feature training using several low-illumination image signals. Shen et al. [34] analyzed the performance of the MSR algorithm from the perspective of CNNs and proposed a method for enhancing low-illumination images using the MSR network with a CNN architecture. Tao et al. proposed a learning framework based on a low-light CNN (LLCNN); their technique first required training on low-illumination images of various kernels before producing the enhanced image using multilevel features [38]. Park et al. proposed a dual self-coding network model based on retinex theory [30], which combined a stacked autoencoder and a convolutional autoencoder to perform low-light enhancement and noise reduction with satisfactory results. Inspired by multiple image fusion methods [2], Cai et al. proposed a method for training a single image enhancer using a CNN. After a large-scale multiexposure image dataset was created, the low-illumination image was enhanced through end-to-end CNN training on low-contrast and high-contrast image datasets. However, the above methods share some shortcomings, including local overenhancement due to uneven illumination at the time of image acquisition and the lack of adaptability of the parameter settings.

According to the theory of image formation, an image is formed when the light rays emitted from the surfaces of the objects in the scene reach the imaging unit. Usually, a digital image can be thought of as a two-dimensional function $F(x,y)$, whose value is the brightness value of the image at the current coordinate point (x,y) . $F(x,y)$ consists of the product of the illumination of the incident light $I(x,y)$ in the scene and the transmission component $R(x,y)$ of the object surfaces. The expression of the basic theoretical model is as follows:

$$F(x,y) = I(x,y)R(x,y) \quad (1)$$

This model is called the illumination-reflection model, and its spatial relationship is shown in Fig. 1.

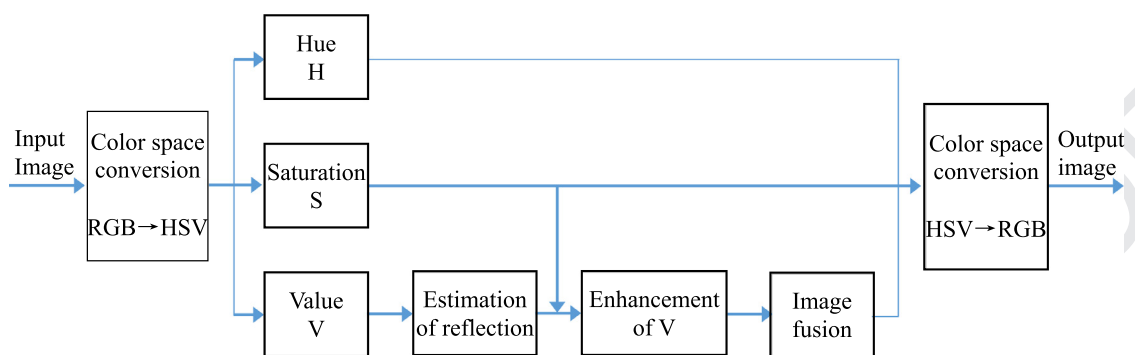
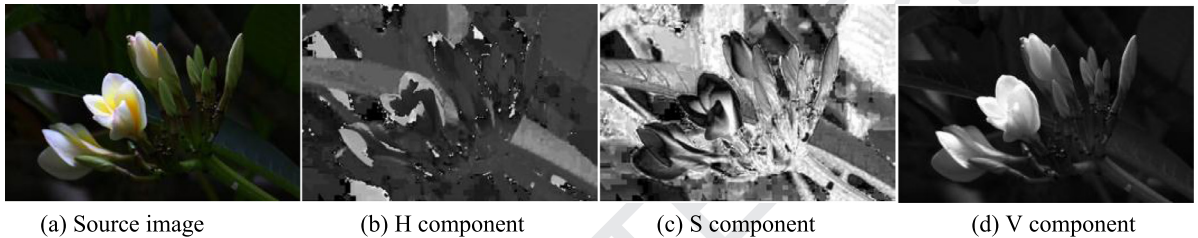
The incident light intensity depends on the light source. The distribution function $I(x,y)$ varies mildly with space. The lines of the spectrum in the space-frequency domain are largely concentrated in the low-frequency band, reflecting the environmental conditions for imaging. The lines of the spectrum of the reflected light $R(x,y)$ are largely concentrated in the high-frequency band, which is relatively wide, reflecting the characteristics of the object itself. Therefore, if a method can be found to estimate $I(x,y)$ from $F(x,y)$ and separate the reflection component from the total illumination, the influence of the incident component on the image quality can be mitigated, thus achieving the purpose of image enhancement.

3. Our method

Combining the strengths of the color-space transformation algorithm and the multiscale decomposition technique, the proposed method enhances images via image fusion. First, the original RGB image is converted into HSV color space, and component V is extracted. Then, the parameters of the adaptive enhancement function are adjusted according to the distribution of the estimated illumination component to obtain two images. Next, image fusion is used to extract the significant information from the image to enhance the V component. Finally, the image is converted back from HSV space to RGB space. The process is shown in Fig. 2.

3.1. Space conversion

The human eye is more sensitive to brightness than to color; therefore, the correction of the illumination component is of crucial importance for an algorithm designed to correct images acquired under uneven illumination. For color images, if the correction is performed directly on the red (R), green (G), and blue (B) channels, it is difficult to ensure that all channels are enhanced or attenuated according to a proper ratio, which often leads to color distortion in the image after correction processing. Given that HSV color space better suits the visual characteristics of the human eye and that the hue

**Fig. 2.** Framework of the proposed algorithm.**Fig. 3.** Example of the conversion from RGB space to HSV space.

117 (H), saturation (S), and brightness (V) in the color space are independent of each other, the manipulation of the brightness
 118 component, V, does not affect the color information of the image. Therefore, in this paper, a color image is corrected in HSV
 119 color space [36]. The mathematical expression of the conversion from RGB space to HSV space is as follows:

$$\begin{cases} V = \max(R, G, B) \\ S = 1 - \min(R, G, B)/V \\ H = \begin{cases} 60 \times (G - B)/(V - \min(R, G, B)) & \text{if } V = R \\ 120 + 60 \times (B - R)/(V - \min(R, G, B)) & \text{if } V = G \\ 240 + 60 \times (R - G)/(V - \min(R, G, B)) & \text{if } V = B \end{cases} \end{cases} \quad (2)$$

120 where R, G, and B are the red, green and blue channels in RGB color space, and H, S, and V are the hue, saturation and
 121 brightness channels in HSV color space, respectively.

122 After the conversion from RGB space to HSV space, the subimages $I_h(x, y)$, $I_s(x, y)$, and $I_v(x, y)$ corresponding to each
 123 component value (H, S, V) are obtained, as shown in Fig. 3.

124 3.2. Estimation of the reflection component

125 Because the multiscale Gaussian function method can effectively compress the dynamic range and accurately estimate the
 126 illumination component of a scene, this method is used to extract the illumination components from images with uneven
 127 illumination. The Gaussian function is used in the following form:

$$G(x, y) = \lambda e^{-\frac{x^2+y^2}{\sigma^2}} \quad (3)$$

128 where σ is the scale parameter. The smaller the value of the scale parameter is, the larger the dynamic range of the image
 129 to be compressed and the clearer the part. λ is a normalization factor that ensures that the Gaussian function satisfies
 130 $\int \int G(x, y) dx dy = 1$. Performing the convolution operation on the image with the Gaussian function provides an estimate of
 131 the value of the illumination component. The result is as follows:

$$I_{v-g}(x, y) = I_v(x, y) * G(x, y) \quad (4)$$

132 where $I_v(x, y)$ is the input image and $I_{v-g}(x, y)$ is the estimated value of the illumination component.

133 To balance the global and local natures of the extracted illumination value, a multiscale Gaussian function is employed
 134 to extract the illumination components of the scene using Gaussian functions of several scales, and weights are assigned to
 135 the functions to ultimately obtain the estimated values of the illumination components. The expression is as follows:

$$I_{v-g}(x, y) = \sum_{i=1}^N \theta_i [I_v(x, y) * G_i(x, y)] \quad (5)$$

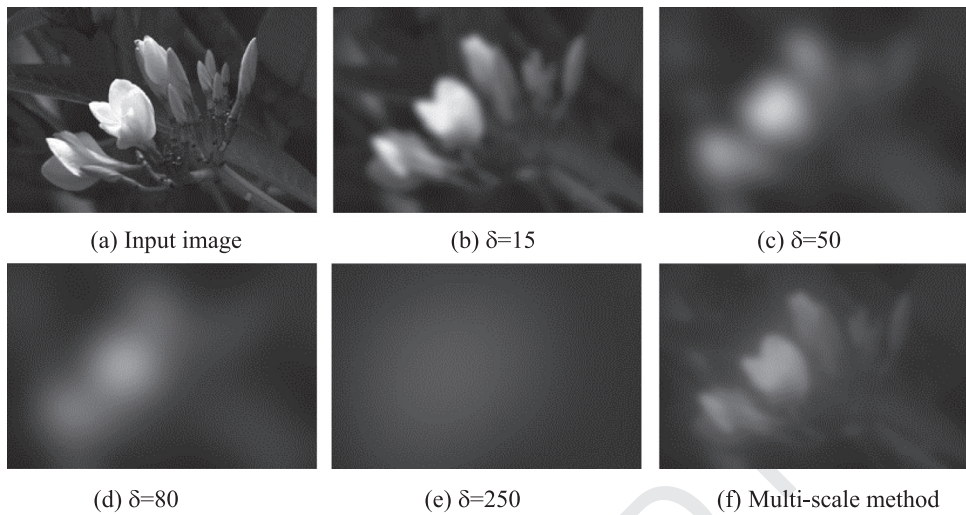


Fig. 4. Extraction of the illumination component on a single scale and multiple scales.

where θ_i is the weight coefficient of the illumination component extracted by the Gaussian function with i scales and N is the number of scales used. Considering the balance between the precision of the illumination component extraction and the amount of computation, this paper uses $N=3$. In other words, to extract the values of the illumination components, Gaussian functions with three values of scale factor σ (i.e., 15, 80, and 250) are used, and the weight coefficient of the illumination component extracted on each scale is set to 1/3. The three-scale Gaussian function is used to extract the illumination components of the grayscale image, and the results are shown in Fig. 4.

Fig. 4 indicates that the illumination component values extracted by the multiscale Gaussian functions used in this paper can effectively describe the illumination changes without detailed information, which adequately meets the requirements of illumination component extraction and demonstrates that the proposed method based on the multiscale Gaussian function can effectively extract the illumination component of a scene.

3.3. Adaptive brightness enhancement

After the illumination component of the scene is extracted, the illumination enhancement function can be constructed according to the distribution profile of the illumination component. The illumination values of the overilluminated areas will decrease, and the illumination values of the underilluminated areas will increase. To achieve this result, this paper proposes an adaptive brightness correction method based on the Weber-Fechner law, which adaptively adjusts the parameters of the enhancement function according to the distribution profile of the illumination components of the image, thus improving the overall quality of images with uneven illumination.

According to the Weber-Fechner law, the subjective brightness perceived by the human eye is created when the light rays reflected from the object hit the retina of the human eye and stimulate the optic nerves. The relationship between the subjective brightness perception I'_v and the objective brightness I_v can be described as logarithmically linear, that is:

$$I'_v = \beta \lg(I_v) + \beta_0 \quad (6)$$

where β and β_0 are constants and $\lg(\cdot)$ is the logarithmic transformation. The relationship between subjective brightness and objective brightness is shown in Fig. 5(a). The curve is used to adjust the tone of the image to be enhanced. To avoid the increased computational burden required by the logarithm operation, a simple function is used in practice to fit the curve in Fig. 5(a):

$$I'_v = \frac{I_v(255 + k)}{I_v + k} \quad (7)$$

where the value 255 is the gray level of the 8-bit image and k is the adjustment coefficient. The smaller the value of k is, the greater the extent of the adjustment. Fig. 5(b)-(f) are the adjustment curves with k values of 25, 50, 75, 100, and 128, respectively, which indicate that the magnitude of image enhancement decreases with increasing k .

To limit the extent of image enhancement and avoid overenhancement, the following enhancement formula used is:

$$I'_v = \frac{I_v(255 + k)}{(\max(I_v, I_{v,g}) + k)} \quad (8)$$

where I'_v is the enhanced image, I_v is the image before enhancement, and $I_{v,g}$ is the reflection component estimated according to I_v .

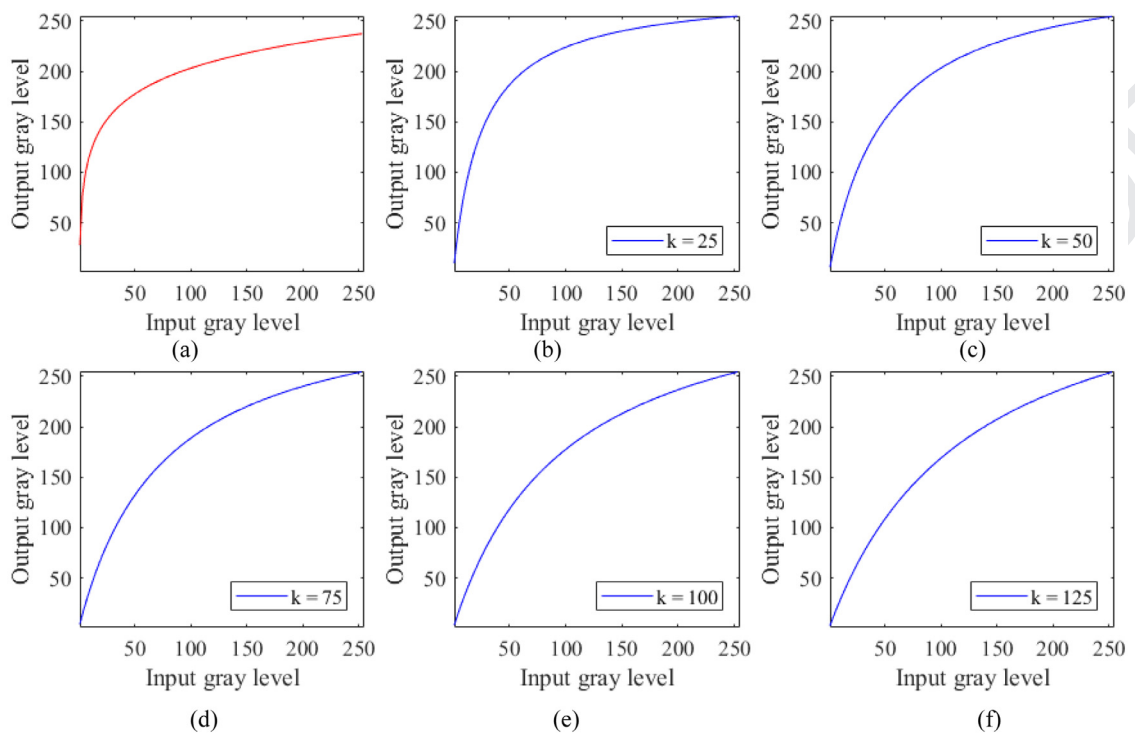


Fig. 5. Brightness adjustment curves.

166 In the experiment, k was automatically obtained according to the average value of the saturation component image I_s , as
167 follows:

$$k = \alpha \times \bar{I}_s = \alpha \times \frac{1}{W} \sum_{i=1}^W I_s \quad (9)$$

168 where α is the weight coefficient, \bar{I}_s is the average value of the image I_s , and W is the total number of pixels in image I_s .
169

170 The output image and histogram vary with α in the manner shown in Fig. 6. As α decreases, the brightness of the
171 output image is enhanced, and the distribution of the grayscale histogram is widened, which indicates that both the overall
brightness and the contrast of the adjusted image are improved.

172 3.4. Image fusion

173 One effective method for obtaining the distinctive features of images is fusing the key information from multiple subim-
174 ages using an image fusion technique. Although multiresolution methods, such as wavelet transform and Laplacian pyramid
175 decomposition, can achieve good results in low-noise image fusion, they have extensive computational requirements and
176 are susceptible to the interference of noise. Fig. 7 shows the fusion results using four-scale Haar wavelets and three-scale
177 Laplacian pyramid decomposition. As shown in Fig. 7(c) and (d), the block effect exists in the image fused with the wavelet
178 transform method, and the Laplacian pyramid method results in the discontinuous effect (the obvious areas are marked by
179 red boxes).

180 Fusion algorithms that are not based on multiscale decomposition do not perform multiscale decomposition on the orig-
181 inal images; instead, they obtain the fused image by simply calculating the weighted addition of the source images, that is:
182

$$F = \sum_{i=1}^N \omega_i S_i \quad (10)$$

183 where F is the fused image, S_i is the source image to be fused, and ω_i is the weighting coefficient.

184 As the images to be fused have similar overall information, the proposed image fusion algorithm determines the weight-
185 ing coefficients using principal component analysis (PCA). Through PCA, the principal components of similar images are
186 identified by calculating the feature vectors of the source images and the corresponding feature values, and the weights of
187 the subimages to be fused are determined according to the principal components. The process is shown in Fig. 8.

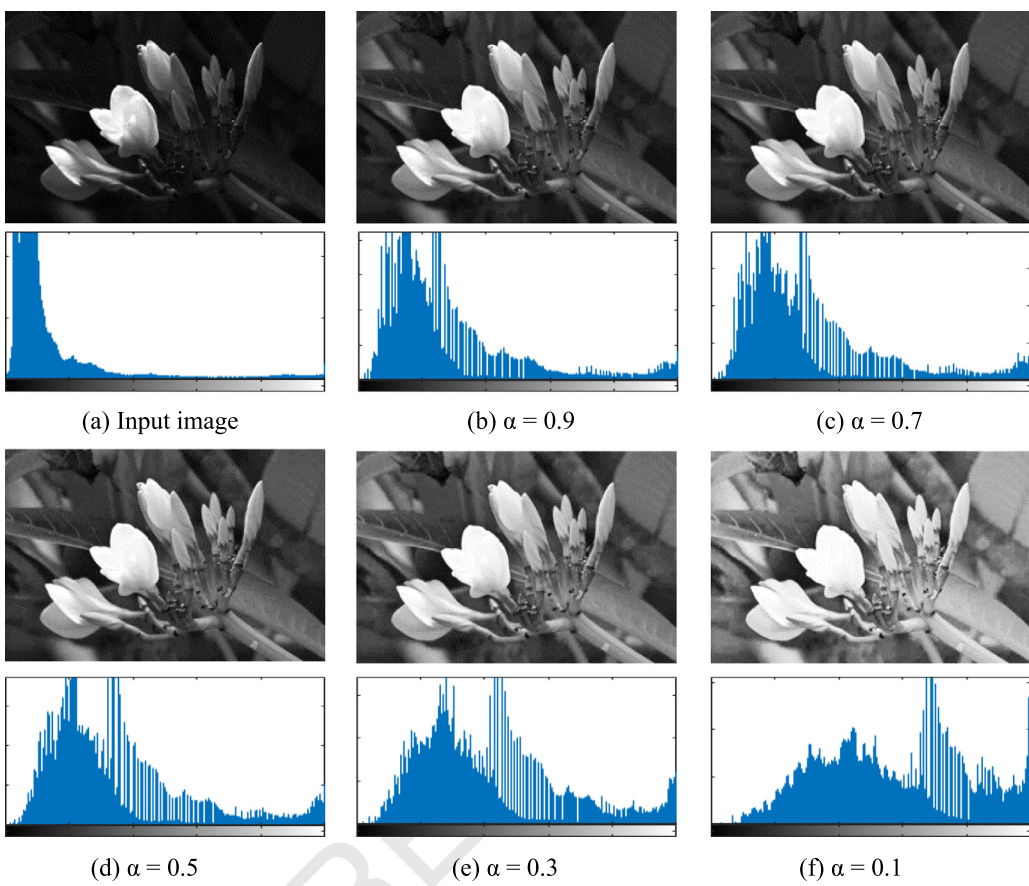


Fig. 6. Variation in the output image and histogram with α .

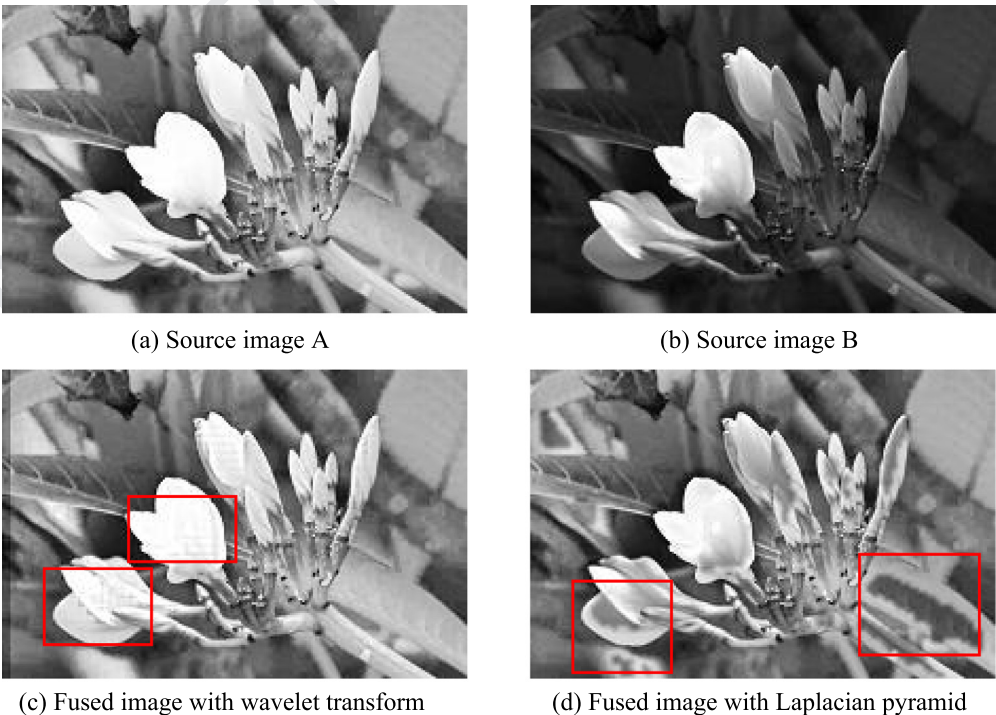
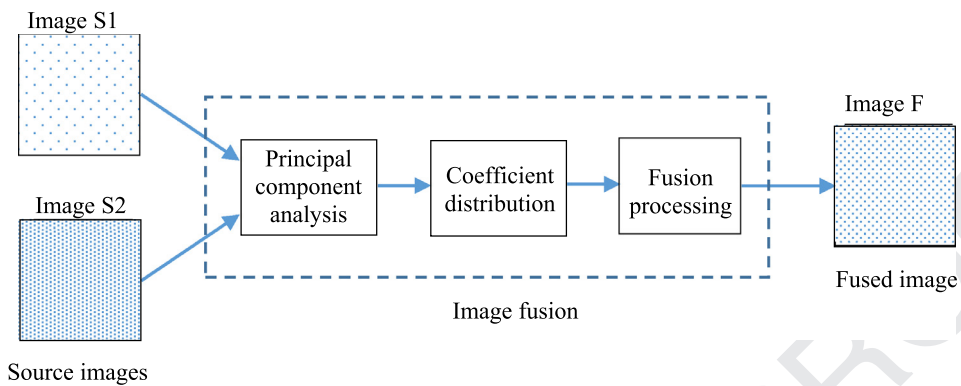


Fig. 7. Image fusion based on multiscale decomposition.

**Fig. 8.** Image fusion process based on PCA transformation.

188 For two source images, S_1 and S_2 , each image is regarded as an n -dimensional vector denoted as X_p , $p = 1, 2$. The steps
189 of the image fusion process are as follows:

190 (1) Construct matrix X using the source images.

$$X = \begin{bmatrix} x_{11} & x_{21} \\ x_{12} & x_{22} \\ \vdots & \vdots \\ x_{1n} & x_{2n} \end{bmatrix} = [X_1, X_2] \quad (11)$$

191 (2) Calculate the covariance matrix C of the data matrix X .

$$C = \begin{bmatrix} \sigma_{11}^2 & \sigma_{12}^2 \\ \sigma_{21}^2 & \sigma_{22}^2 \end{bmatrix} \quad (12)$$

192 $\sigma_{i,j}^2$ is the covariance of the image, which satisfies:

$$\sigma_{i,j}^2 = \frac{1}{n} \sum_{l=1}^n (x_{i,l} - \bar{x}_i)(x_{j,l} - \bar{x}_j) \quad (13)$$

193 \bar{x}_i is the average grayscale value of the i th source image.

194 (3) Create the eigenvalue formula $|\lambda I - C| = 0$ and calculate the eigenvalue (λ_1, λ_2) and feature vector (ξ_1, ξ_2) of the
195 covariance matrix C , where ξ_i is a vector $\begin{bmatrix} \xi_{i1} \\ \xi_{i2} \end{bmatrix}$ whose size is 2×1 .

196 (4) Select a large eigenvalue.

$$p = \arg \max (\lambda_p) \quad p = 1 \text{ or } 2 \quad (14)$$

197 (5) Calculate the weight coefficient using the feature vector corresponding to the largest eigenvalue.

$$\omega_1 = \frac{\xi_{i1}}{\xi_{i1} + \xi_{i2}} \text{ and } \omega_2 = \frac{\xi_{i2}}{\xi_{i1} + \xi_{i2}} \quad (15)$$

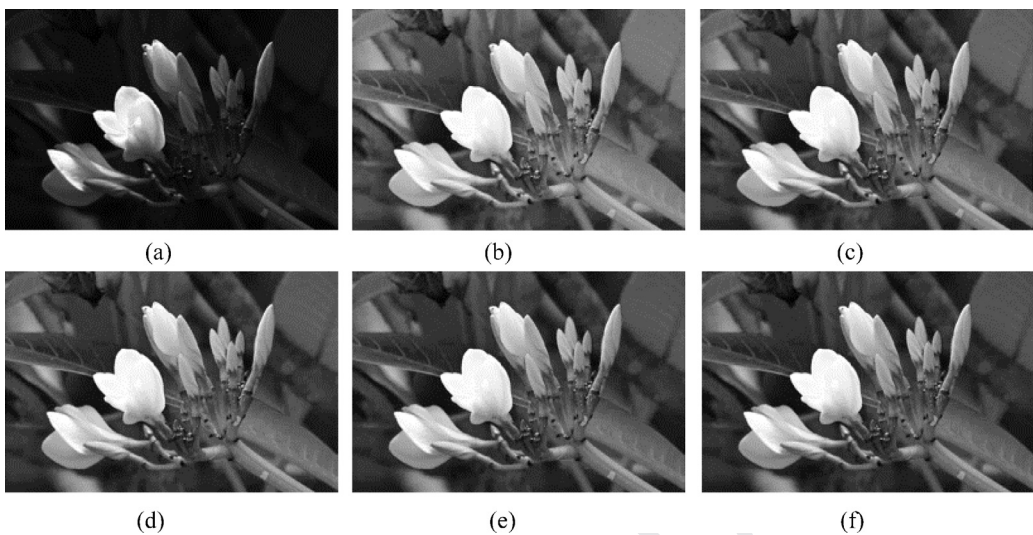
198 (6) Calculate the fused image F .

$$F = \omega_1 S_1 + \omega_2 S_2 \quad (16)$$

199 In the PCA method, image fusion is performed based on the correlation between the selected component images. The
200 data of the shared features are compressed, while the data of unique features are augmented. The effect of fusion is shown
201 in Fig. 9, where (a) is the original image, (b)–(f) are the fused images with different combinations of $(\alpha = 0.1, \alpha = 1)$, $(\alpha =$
202 $0.2, \alpha = 0.9)$, $(\alpha = 0.3, \alpha = 0.8)$, $(\alpha = 0.4, \alpha = 0.7)$, and $(\alpha = 0.5, \alpha = 0.6)$, respectively. As seen in the figure, the amount of
203 image information decreases gradually from high to low, so in the following experiments, the parameters of the two images
204 used for image fusion are set to $(\alpha = 0.1, \alpha = 1)$.

205 **3.5. Converting to RGB space**

206 The image is converted to RGB space using the formula.

**Fig. 9.** Image fusion based on PCA.

207 4. Experiment and analysis

208 To verify the effectiveness of the algorithm, a test platform based on a desktop computer (Intel (R) Core (TM) i7-6700 CPU
 209 @ 3.4 GHz, 16 G RAM and Windows 10 operating system) was built. The test software was MATLAB 2017b. The experimental
 210 images included urban streetscapes, natural scenery, and indoor images. All images shared one trait: the difference between
 211 the maximum brightness and minimum brightness was relatively large. The adaptive low-illumination image enhancement
 212 algorithm based on multiscale fusion was implemented as follows:

Algorithm

- Step 1: Enter a low-illumination image I .
- Step 2: Convert the image from RGB space to HSV space using Formula (1) to obtain the brightness map I_v , saturation map I_s , and tone map I_h .
- Step 3: Extract the illumination component from I_v using Formula (5) to obtain image $I_{v,g}$.
- Step 4: Let $\alpha_1 = 0.1$ and $\alpha_2 = 1$ and obtain the enhanced images I'_{v1} and I'_{v2} using Formulas (8) and (9), respectively.
- Step 5: Calculate the covariance values of I'_{v1} and I'_{v2} using Formula (12).
- Step 6: Calculate the eigenvalue and feature vector of covariance matrix C .
- Step 7: Calculate the weight coefficient using Formula (15).
- Step 8: Obtain the fused image using Formula (16).
- Step 9: Use Image F as the lamination component to merge with I_s and I_h and convert the image into image J in RGB space.
- Step 10: Output the enhanced color image J .

213 Some of the experimental results are shown in Fig. 10. The six sets of experimental images were named 'Plaque', 'Road',
 214 'Wood', 'Deer', 'Girl', and 'Plate'. Fig. 9 demonstrates that crisp images with naturalistic colors could be obtained after image
 215 enhancement processing, irrespective of whether the source image was a distant scene or a close-up scene, which proves
 216 the effectiveness and adaptability of the proposed method.

217 In the following sections, the results of several experiments will be presented. Several experimental images were pro-
 218 cessed by multiple mainstream image enhancement algorithms to evaluate the effectiveness of the proposed algorithm. The
 219 quality of each enhanced image was evaluated from three perspectives: subjective visual evaluation, objective quantitative
 220 analysis, and computational complexity.

221 4.1. Subjective visual evaluation

222 (1) Comparison with several conventional image enhancement algorithms

223 Fig. 11 shows the experimental results of image enhancement after the original images were processed by the proposed
 224 algorithm and several conventional algorithms. Fig. 11(a) is the original image, and Fig. 11(b)–(h) are the processing results
 225 of linear transformation, histogram equalization (HE), AHE, homomorphic filtering, wavelet transformation, retinex method,
 226 and the proposed algorithm, respectively. The images shown in the third and sixth rows are the enlarged details indicated
 227 in Fig. 11(a). As shown, the images in Fig. 11(b)–(h) differ in terms of image quality. The images in Fig. 11(c), (e), and (g)
 228 have obviously greater contrast with many accentuated details. However, these images exhibit serious hue deviations. The
 229 image in Fig. 11(f) is not flawed by hue deviation; however, the improvement in contrast is not obvious (the image can
 230 even be regarded as blurred). Fig. 11(b), (d), and (h) have good overall quality. Moreover, linear transformation caused image

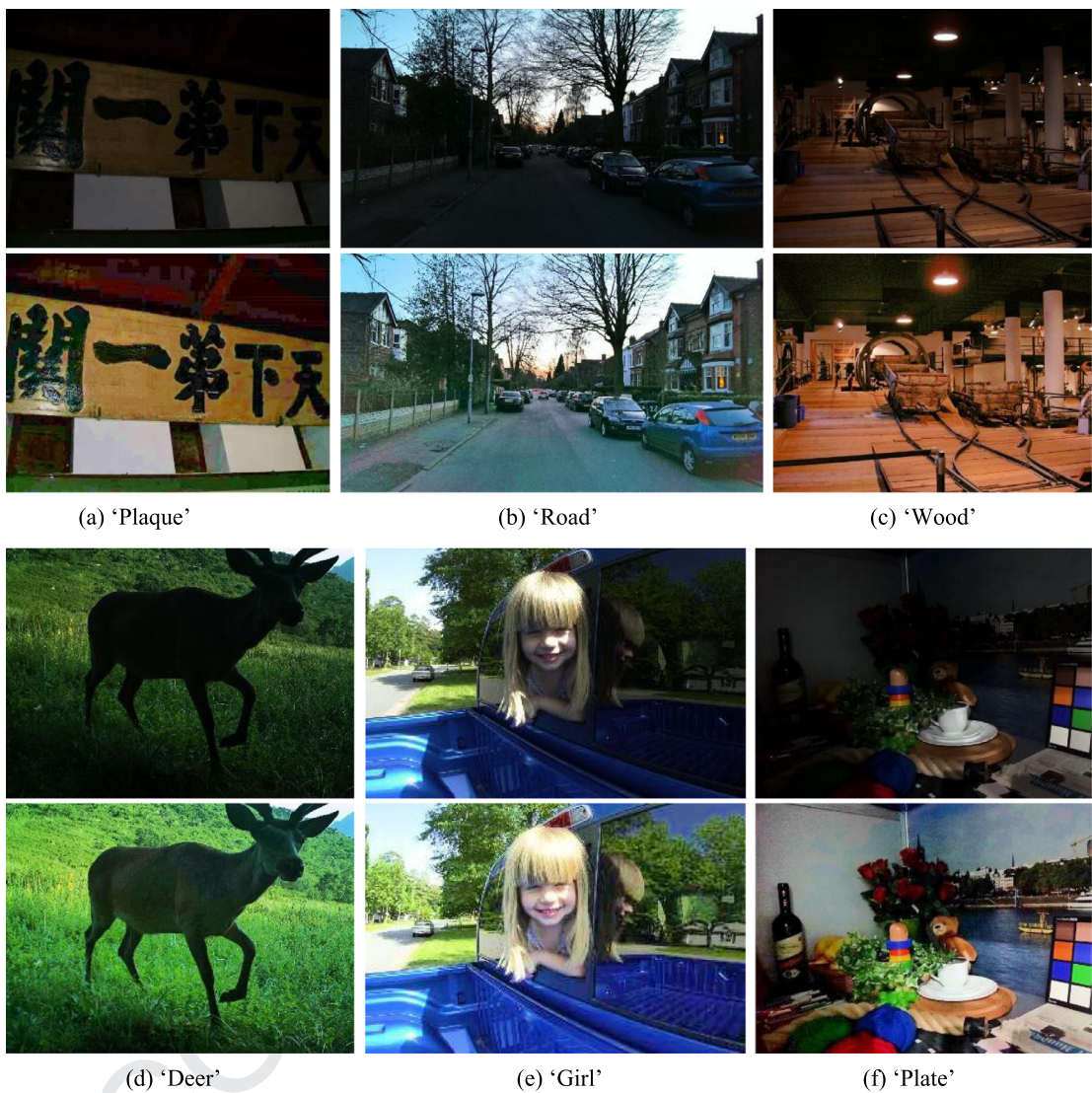


Fig. 10. Part of the experimental results.

231 overenhancement, while the images processed by the AHE method are significantly darker than the others. By contrast, the
 232 method proposed in this paper significantly improved both color and detail and outperformed the other algorithms in terms
 233 of visual effect.

234 (2) Comparison with several new algorithms

235 The images 'Night', 'Building', and 'Officers' were used to compare the proposed algorithm with several advanced
 236 algorithms that have been proposed in recent years. The experimental results are shown in Figs. 12–14. Panel (a) shows
 237 the original images and some zoomed-in areas. Panels (b)–(h) show the experimental results of image enhancement after
 238 the original images were enhanced using the proposed algorithm and several new algorithms, namely, EFF [47], CVC
 239 [3], LDR [22], DCP [35], MSRCP [31] and SRIE [10]. Zoomed-in areas are shown in the figure below. After implementing
 240 image enhancement, all the algorithms significantly improved the overall visibility and contrast of each image. A close
 241 examination reveals the differences between the algorithms. For the 'Night' and 'Building' images, CVC and LDR achieved
 242 only a modest improvement and amplified the noise in dark areas. In addition, CVC failed to restore the colors of the pixels
 243 in low-illumination areas. MSRCP and SRIE achieved good results in terms of detail enhancement, but the resulting images
 244 were flawed due to low brightness. EFF, DCP, and the proposed algorithm produced better results than MSRCP in terms
 245 of color and brightness enhancement. DCP obviously overenhanced the edges of objects, and EFF was outperformed by
 246 the proposed algorithm. For the 'Officers' image, EFF, DCP, SRIE, and the proposed algorithm achieved good overall quality.
 247 The details in the zoomed-in areas show that DCP produced a high level of noise due to overenhancement at the edges of

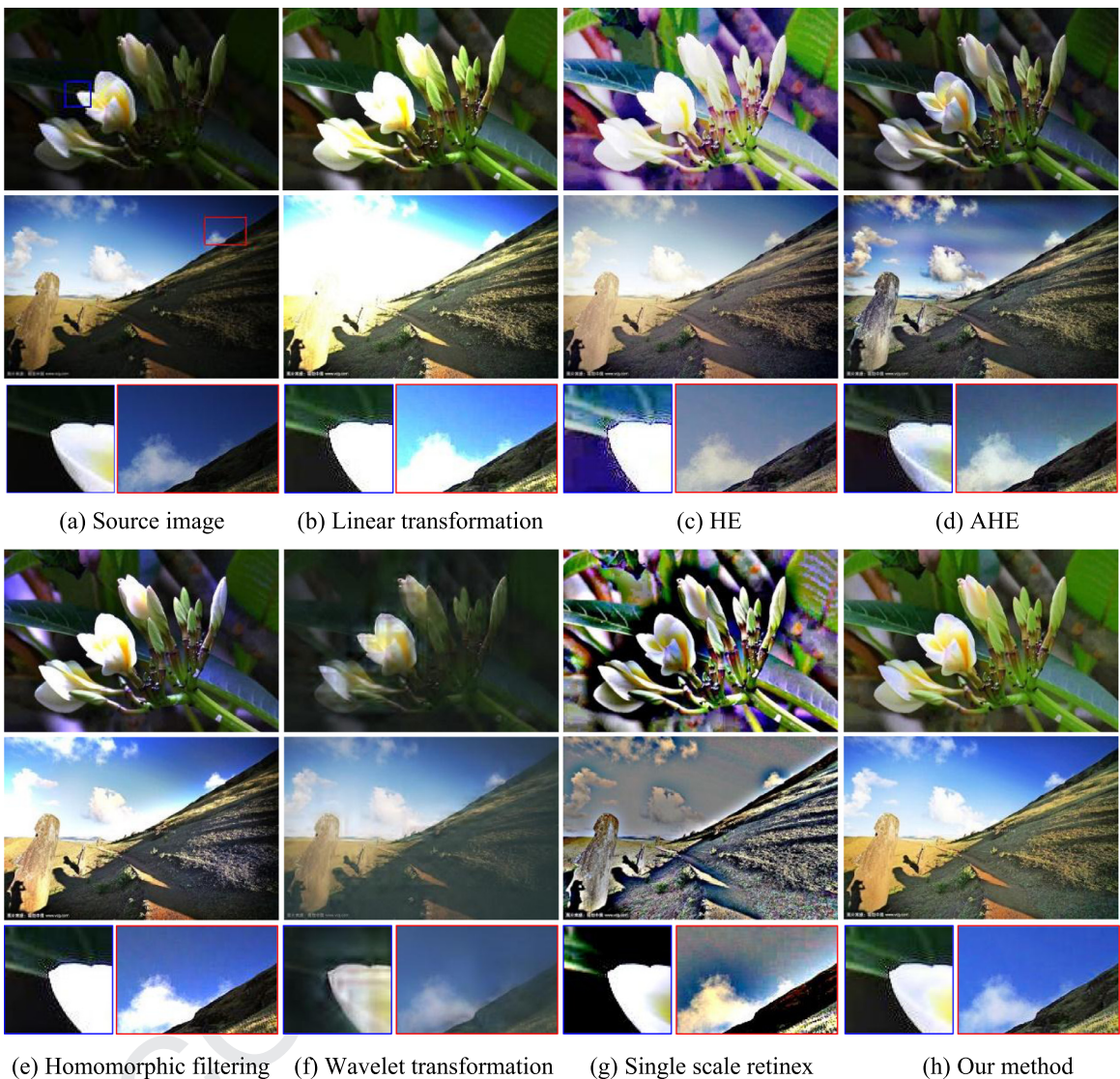


Fig. 11. Comparison of the proposed algorithm with several conventional algorithms.

248 objects. Moreover, the images enhanced by EFF do not have bright colors, and unevenness can be seen in the alternating
249 bright-dark areas on the images enhanced by SRIE. Overall, the proposed algorithm achieved better results than the other
250 algorithms in terms of resolution, contrast, and color.

251 The proposed algorithm significantly augmented the objects that needed to be accentuated without excessively amplifying
252 the noise in dark areas, and it did not overenhance the images.

253 4.2. Objective quantitative analysis

254 As different methods have different image enhancement focuses, sufficient objectivity is difficult to achieve in a subjective
255 assessment. Therefore, an objective assessment is performed using information entropy and an average gradient to further
256 assess the effectiveness of the selected algorithms [27]. The physical meanings are as follows [23,25,43].

257 (1) Information entropy (IE). A still image is considered an information source with random output. Source symbol set
258 A is defined as the set of all possible symbols $\{a_i\}$, and the probability of source symbol a_i is $P(a_i)$. Thus, the average
259 amount of information contained in this image is expressed as follows:

$$H = - \sum_{i=1}^L P(a_i) \log_2 P(a_i) \quad (17)$$



Fig. 12. Comparison with state-of-the-art methods on the 'Night' image.

According to the theory of entropy, the larger the value of IE is, the larger the amount of information in the image and the richer the detailed information in the image.

(2) Average gradient (AG). The AG reflects the ability to express the details of an image and can be used to measure the relative clarity of the image. AG is formulated as:

$$AG = \frac{1}{M \times N} \sum_{i=1}^M \sum_{j=1}^N \sqrt{\frac{(\partial f / \partial x)^2 + (\partial f / \partial y)^2}{2}} \quad (18)$$

where M and N are the width and height of the image, respectively, $\partial f / \partial x$ represents the horizontal gradient, and $\partial f / \partial y$ represents the vertical gradient.

To improve the significance of the data, a comprehensive evaluation parameter was set in the experiment so that the average values of different sets of test data could be presented in a consistent manner:

$$\bar{Y} = \frac{n}{\sum_{i=1}^n Y_i} \quad (19)$$

where n is the sample size, Y_i is the result of testing on a certain sample, and \bar{Y} is the average value.

The IE and AG of the images in Figs. 11–13 are shown in Table 1: the best values are underlined.

We also used other images for comparison and verification. The experimental images include both indoor and outdoor images with low illumination and uneven illumination (a few examples are shown in Fig. 15), and their corresponding assessment data (IE and AG) are shown in Tables 2 and 3, respectively.

The data in Tables 2 and 3 indicate that the images processed by various methods were improved in terms of both IE and AG, among which EFF, MSRCP and the proposed method achieved relatively high values. Although the IE or AG values of individual images processed by MSRCP were higher than those of the method proposed in this paper, the comprehensive performance of the method in this paper is much better than that of the other methods.

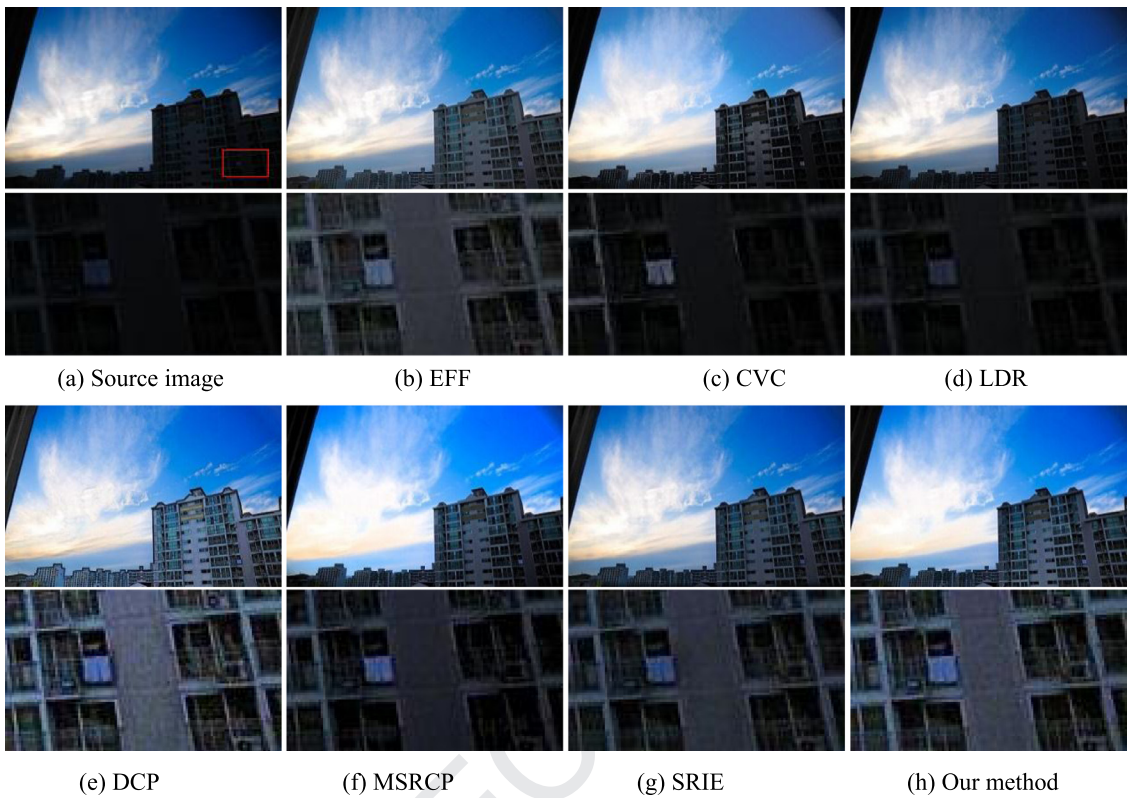


Fig. 13. Comparison with state-of-the-art methods on the 'Building' image.

Table 1
The assessment results on the 'Night', 'Building' and 'Officers' images.

Image name	Metric	Unprocessed	EFF	LDR	MSRCP	SRIE	Our method
Image 'Night'	IE	5.63	7.03	7.08	7.05	6.80	<u>7.50</u>
	AG	2.10	7.13	6.97	7.08	6.68	<u>10.54</u>
Image 'Building'	IE	7.73	7.84	7.86	7.79	<u>7.90</u>	7.87
	AG	1.85	3.01	2.18	3.14	3.08	<u>3.40</u>
Image 'Officers'	IE	6.13	7.02	6.38	7.36	7.07	<u>7.44</u>
	AG	0.85	1.91	1.04	2.39	2.44	<u>3.52</u>
Average value	IE	6.49	7.29	7.10	7.40	7.25	<u>7.60</u>
	AG	1.60	4.01	3.39	4.20	4.06	<u>5.82</u>

277 4.3. Computational complexity

278 The images in Fig. 15 are used for experiments to test the processing speed of the proposed method, and each group of
279 experiments is repeated ten times to obtain the average value. As shown in Table 4, as the number of pixels in the image
280 increases, the operation time increases, and the time required to process images with 795×1200 pixels exceeds 1 s.

281 In addition, images with 600×400 , 800×600 , 1024×768 , 1600×1200 and 2048×1536 pixels are used for comparison
282 with other methods. Table 5 shows that NPE and SRIE exhibit the lowest computational efficiency in processing a single
283 image. When processing an image with 2048×1536 pixels, the processing times for NPE and SRIE are 89 s and 242 s,
284 respectively. The main reason for this result is that iteration methods have high computational complexity and can com-
285 pute only limited size images. The proposed method is comparable to the MSRCP method, and the majority of the time is
286 consumed by the three scales of Gaussian filtering.

287 The results of the above analysis indicate that it is necessary to develop an objective quality assessment method that
288 matches the human vision mechanism. The subjective assessment, objective assessment and computational complexity in-
289 dicate that the proposed method can maintain the balance of performance and achieve satisfactory results.

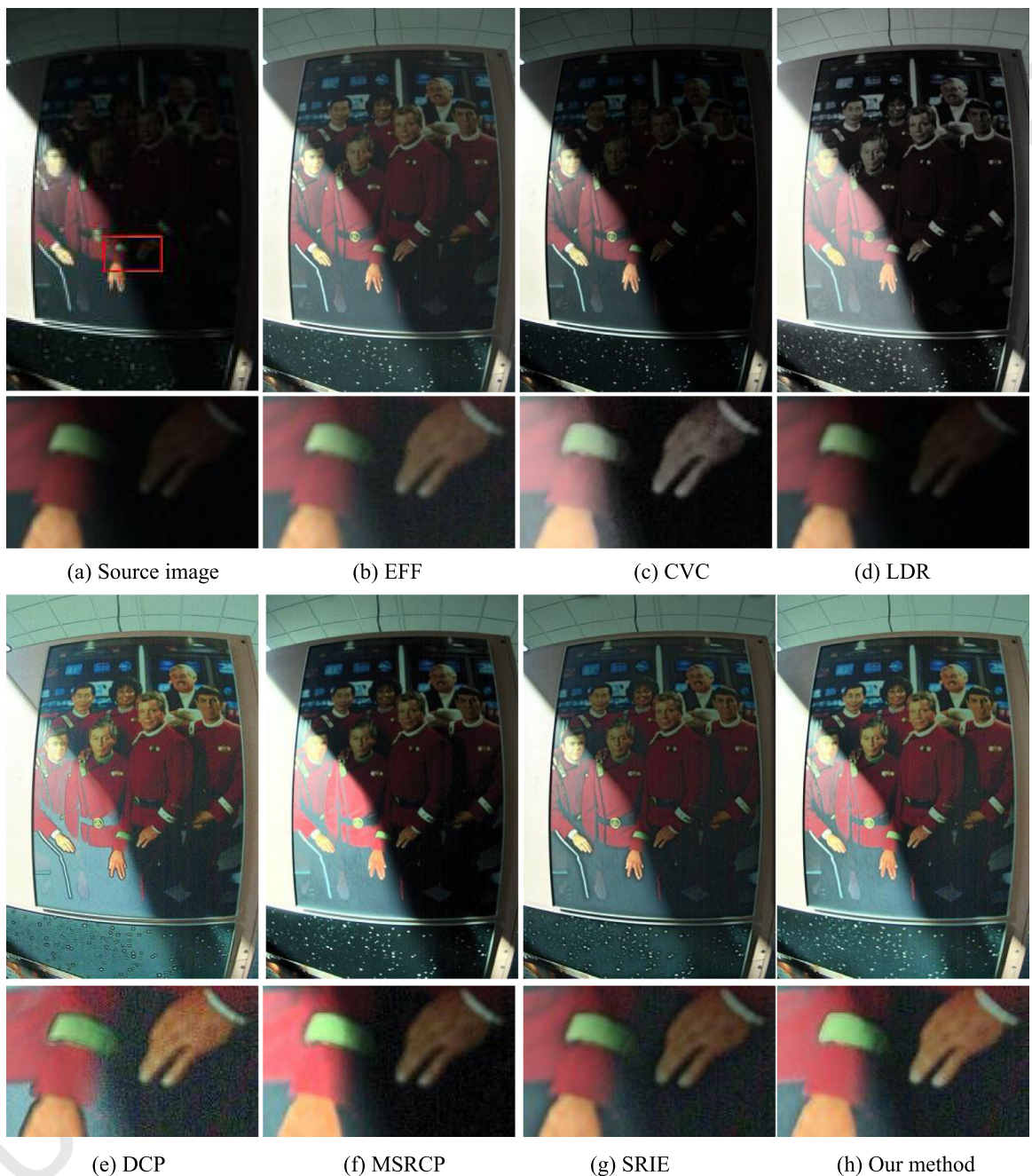
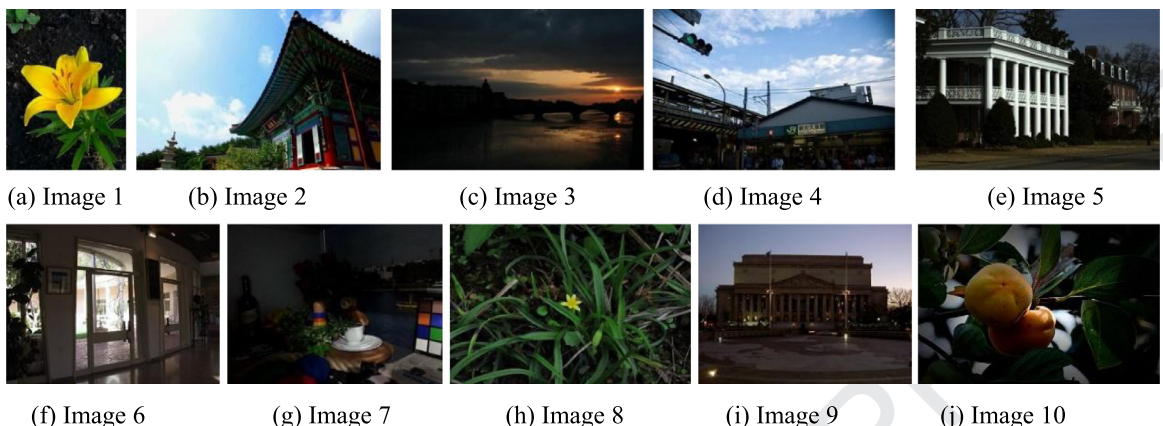


Fig. 14. Comparison with state-of-the-art methods on the 'Officers' image.

290 4.4. Image enhancement under extreme conditions

291 Images with extremely low illumination were also used to evaluate the proposed algorithm, which was a very challenging
292 task. The experimental results are shown in Fig. 16.

293 The original images are in the first row, and the enhanced images are shown in the second row. The outcome of image
294 enhancement was not satisfactory; however, no block effect was observed in the enhanced images, which makes the images
295 look natural to the human eye.

**Fig. 15.** Examples of the original images used in the experiment.**Table 2**

The information entropy of the images in Fig. 15.

	Unprocessed	EFF	LDR	MSRCP	SRIE	Our method
Image 1	7.03	7.54	7.31	7.62	7.57	<u>7.70</u>
Image 2	7.19	7.61	7.43	7.52	7.40	<u>7.57</u>
Image 3	6.33	7.19	7.03	7.35	7.10	<u>7.42</u>
Image 4	7.52	<u>7.84</u>	7.76	7.51	7.70	7.74
Image 5	7.01	7.48	7.14	7.65	7.55	<u>7.67</u>
Image 6	6.95	7.25	7.13	7.68	7.46	<u>7.70</u>
Image 7	6.06	7.32	6.94	7.33	7.13	<u>7.62</u>
Image 8	6.72	7.50	7.60	<u>7.89</u>	7.35	7.67
Image 9	7.14	7.57	7.63	7.74	7.69	<u>7.80</u>
Image 10	5.96	7.26	6.51	6.96	7.13	<u>7.40</u>
Average value	6.79	7.45	7.24	7.52	7.40	7.62

Table 3

The average gradients of the images in Fig. 15.

	Unprocessed	EFF	LDR	MSRCP	SRIE	Our method
Image 1	2.56	4.67	3.18	5.52	4.53	<u>5.56</u>
Image 2	4.73	7.80	6.12	<u>8.84</u>	5.97	8.28
Image 3	1.19	2.77	1.96	3.01	2.92	<u>3.79</u>
Image 4	4.89	7.14	5.37	7.11	6.13	<u>7.73</u>
Image 5	3.65	5.45	4.28	6.38	5.95	<u>7.14</u>
Image 6	3.80	4.64	4.01	4.92	5.27	<u>5.71</u>
Image 7	2.54	5.36	4.09	5.59	4.82	<u>6.71</u>
Image 8	6.41	10.41	10.71	<u>14.40</u>	9.37	12.96
Image 9	3.06	5.18	4.46	<u>6.76</u>	4.77	6.56
Image 10	1.85	4.30	3.14	<u>4.57</u>	4.05	<u>4.69</u>
Average value	3.46	5.77	4.73	6.71	5.37	<u>6.91</u>

Table 4

Experimental results of computational complexity (Unit: s).

Image index	Size	Time	Image index	Size	Time
Image 1	1632 × 1224	3.72	Image 6	720 × 960	0.83
Image 2	480 × 732	0.42	Image 7	499 × 671	0.43
Image 3	608 × 960	0.63	Image 8	532 × 800	0.49
Image 4	480 × 725	0.41	Image 9	480 × 640	0.39
Image 5	1312 × 2000	4.94	Image 10	795 × 1200	1.07

Table 5

Comparison of different methods on computational complexity (Unit: s).

	600 × 400	800 × 600	1024 × 768	1600 × 1200	2048 × 1536
MSRCP[31]	0.17	0.40	0.88	3.29	7.41
NPE[39]	6.92	13.27	21.33	52.29	89.93
SRIE[10]	7.08	13.61	22.38	101.91	242.02
Proposed	0.34	0.52	0.93	3.19	7.70

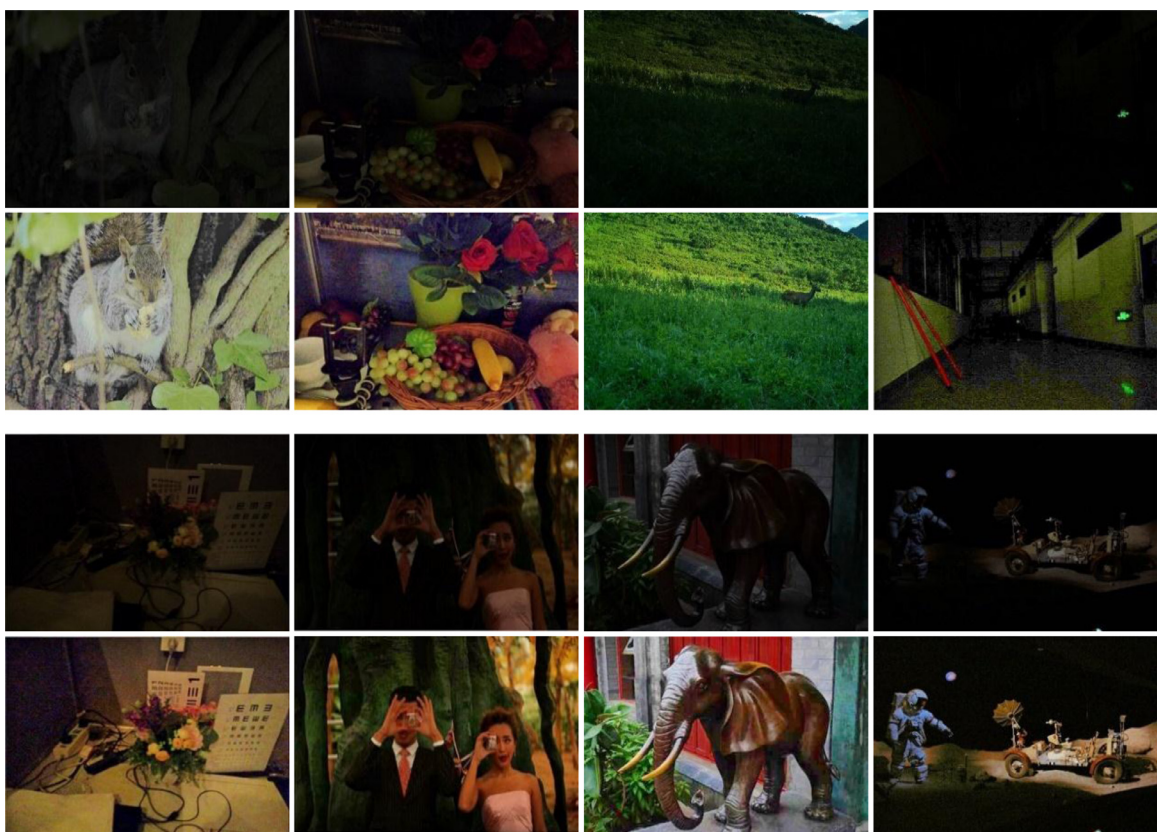


Fig. 16. Examples of enhanced images with extremely low illumination.

296 5. Conclusion

297 This paper addresses two problems of low-illumination image enhancement: local overenhancement due to uneven
 298 illumination and the lack of adaptability in the parameter settings of image enhancement algorithms. A color image correc-
 299 tion method based on nonlinear function transformation was proposed based on the light reflection model and multiscale
 300 theory. First, the original RGB color image was converted to HSV color space, and the V component was used to extract
 301 the illumination component of the scene via the multiscale Gaussian function. Then, a correction function was constructed
 302 based on the Weber-Fechner law, and two images were obtained through an adaptive adjustment of the parameters of the
 303 image enhancement function based on the distribution profiles of the illumination components. Finally, an image fusion
 304 strategy was used to extract the details of the two images. The proposed algorithm balanced the color across the image
 305 better than did the classic algorithms while preserving the image details. Furthermore, the proposed algorithm discovered
 306 details that were previously invisible in the dark areas, significantly improving image quality. This study may lend new
 307 ideas to future studies on the correction of images with uneven illumination. The main weakness of the proposed algorithm
 Q3 is that it cannot be used to enhance video images, and further effort is needed to improve its real-time performance.
 308

Q4

309 Uncited References

310 [20].

311 Acknowledgments

312 This work was supported by the Shandong Provincial Natural Science Foundation (nos. ZR2019MF059, ZR2018BEE032).
 313 National Natural Science Foundation of China (nos. 61403283, 61876099). We also thank AJE (www.aje.com) for its linguistic
 314 assistance during the preparation of this manuscript.

315 References

- 316 [1] H. Alismail, B. Browning, S. Lucey, Robust tracking in low light and sudden illumination changes, in: The Fourth International Conference on 3D Vision,
 317 2016, pp. 389–398.

- [2] J. Cai, S. Gu, L. Zhang, et al., Learning a deep single image contrast enhancer from multi-exposure images, *IEEE Trans. Image Process.* 27 (4) (2018) 2049–2062.
- [3] T. Celik, T. Tjahjadi, Contextual and variational contrast enhancement, *IEEE Trans. Image Process.* 20 (12) (2011) 3431–3441.
- [4] R. Chandrasekharan, M. Sasikumar, Fuzzy Transform for contrast enhancement of non-uniform illumination images, *IEEE Signal Process Lett.* 25 (6) (2018) 813–817.
- [5] S. Chen, A. Ramli, Minimum mean brightness error bi-histogram equalization in contrast enhancement, *IEEE Trans. Consum. Electron.* 49 (4) (2004) 1310–1319.
- [6] Y. Chen, X. Xiao, H. Liu, et al., Dynamic color image resolution compensation under low light, *Optik - Int. J. Light Electron Opt.* 126 (6) (2015) 603–608.
- [7] M.H. Conde, B. Zhang, K. Kagawa, et al., Low-light image enhancement for multiaperture and multitap systems, *IEEE Photonics J.* 8 (2) (2016) 1–25.
- [8] X. Dong, G. Wang, Y. Pang, et al., Fast efficient algorithm for enhancement of low lighting video, in: *IEEE International Conference on Multimedia and Expo*, Washington, 2011, pp. 1–6.
- [9] S. Du, R.K. Ward, Adaptive Region-based image enhancement method for robust face recognition under variable illumination conditions, *IEEE Trans. Circuits Syst. Video Technol.* 20 (9) (2010) 1165–1175.
- [10] X. Fu, D. Zeng, Y. Huang, et al., A weighted variational model for simultaneous reflectance and illumination estimation, in: *IEEE Conference on Computer Vision and Pattern Recognition*, 2016, pp. 2782–2790.
- [11] M. Gharbi, J. Chen, J. Barron, et al., Deep bilateral learning for real-time image enhancement, *ACM Trans. Graph.* 36 (4) (2017) 118.
- [12] X. Guo, Y. Li, H. Ling, LIME: low-light image enhancement via illumination map estimation, *IEEE Trans. Image Process.* 26 (2) (2017) 982–993.
- [13] S. Hao, Z. Feng, Y. Guo, Low-light image enhancement with a refined illumination map, *Multim. Tools Applica.* 9 (22) (2017) 1–12.
- [14] S. Huang, F. Cheng, Y. Chiu, Efficient contrast enhancement using adaptive gamma correction with weighting distribution, *IEEE Trans. Image Process.* 22 (3) (2013) 1032–1041.
- [15] T. Huynh-The, B. Le, S. Lee, et al., Using weighted dynamic range for histogram equalization to improve the image contrast, *EURASIP J. Image Video Process.* 1 (1) (2014) 44.
- [16] D. Jobson, Z. Rahman, G. Woodell, Properties and performance of a center/surround Retinex, *IEEE Trans. Image Process.* 6 (3) (1997) 451–462.
- [17] D. Jobson, Z. Rahman, G. Woodell, A multiscale Retinex for bridging the gap between color images and the human observation of scenes, *IEEE Trans. Image Process.* 6 (7) (2002) 965–976.
- [18] J. Kim, L. Kim, S. Hwang, An advanced contrast enhancement using partially overlapped sub-block histogram equalization, *IEEE Trans. Circu. Syst. Video Technol.* 11 (4) (2011) 475–484.
- [19] T. Kim, J. Paik, B. Kang, Contrast enhancement system using spatially adaptive histogram equalization with temporal filtering, *IEEE Trans. Consum. Electron.* 44 (1) (1998) 82–87.
- [20] Y. Kim, Contrast enhancement using brightness preserving bi-histogram equalization, *IEEE Trans. Consum. Electron.* 43 (1) (1997) 1–8.
- [21] E. Land, J. McCann, Lightness and retinex theory, *J. Opt. Soc. Am.* 61 (1) (1971) 1–11.
- [22] C. Lee, C. Lee, C.S. Kim, Contrast enhancement based on layered difference representation of 2D histograms, *IEEE Trans. Image Process.* 22 (12) (2013) 5372–5384.
- [23] H. Li, T. Han, J. Wang, et al., A real-time image optimization strategy based on global saliency detection for artificial retinal prostheses, *Inform. Sci.* 415 (2017) 1–18.
- [24] L. Li, Y. Si, Z. Jia, Medical image enhancement based on CLAHE and unsharp masking in NSCT domain, *J. Med. Imag. Health Inform.* 8 (3) (2018) 431–438.
- [25] P. Liu, J. Guo, K. Chamnongthai, et al., Fusion of color histogram and LBP-based features for texture image retrieval and classification, *Inform. Sci.* 390 (2017) 95–111.
- [26] S.C. Liu, S. Liu, H. Wu, et al., Enhancement of low illumination images based on an optimal hyperbolic tangent profile, *Comput. Electri. Eng.* 70 (2017) 1–13.
- [27] K.G. Lore, A. Akintayo, S. Sarkar, LLNet: a deep autoencoder approach to natural low-light image enhancement, *Pattern Recognit.* 61 (2016) 650–662.
- [28] H. Lu, Y. Li, T. Uemura, et al., Low illumination underwater light field images reconstruction using deep convolutional neural networks, *Future Gener. Comput. Syst.* 82 (2018) 82.
- [29] S. Park, B. Moon, S. Ko, et al., Low-light image restoration using bright channel prior-based variational Retinex model, *EURASIP J. Image Video Process.* 2017 (1) (2017) 44.
- [30] S. Park, S. Yu, M. Kim, et al., Dual autoencoder network for Retinex-based low-light image enhancement, *IEEE Access* 6 (2018) 22084–22093.
- [31] A. Petro, C. Sbert, J. Morel, Multiscale Retinex, *Image Process. on Line* 4 (2014) 71–88.
- [32] Z. Rahman, D. Jobson, G. Woodell, Retinex processing for automatic image enhancement, *J. Electron. Imaging* 13 (1) (2004) 100–110.
- [33] H. Shen, S. Sun, B. Lei, et al., An adaptive brightness preserving bi-histogram equalization, *Proced. SPIE* 8005 (1) (2011) 24.
- [34] Shen L, Yue Z, Feng F, et al., MSR-net:low-light image enhancement using deep convolutional network. 2017.
- [35] Z. Shi, M. Zhu, B. Guo, et al., Nighttime low illumination image enhancement with single image using bright/dark channel prior, *EURASIP J. Image Video Process.* 2018 (1) (2018) 13.
- [36] A. Smith, Color gamut transform pairs, in: *ACM SIGGRAPH Computer Graphics*, 1978, pp. 12–19.
- [37] L. Tao, C. Zhu, J. Song, et al., Low-light image enhancement using CNN and bright channel prior, in: *IEEE International Conference on Image Processing*, 2018, pp. 3215–3219.
- [38] L. Tao, C. Zhu, G. Xiang, et al., LLCNN: a convolutional neural network for low-light image enhancement, in: *IEEE Conference on Visual Communications and Image Processing*, 2018, pp. 1–4.
- [39] S. Wang, J. Zheng, H. Hu, et al., Naturalness preserved enhancement algorithm for non-uniform illumination images, *IEEE Trans. Image Process.* 22 (9) (2013) 3538–3548.
- [40] T. Wang, Z. Ji, Q. Sun, et al., Label propagation and higher-order constraint-based segmentation of fluid-associated regions in retinal SD-OCT images, *Inform. Sci.* 358 (2016) 92–111.
- [41] T. Wang, J. Yang, Z. Ji, et al., Probabilistic diffusion for interactive image segmentation, *IEEE Trans. Image Process.* 28 (1) (2019) 330–342.
- [42] T. Wang, J. Yang, Q. Sun, et al., Global graph diffusion for interactive object extraction, *Inform. Sci.* 460 (2018) 103–114.
- [43] W. Wang, X. Yuan, Z. Chen, X. Wu, An adaptive method for low-illumination image enhancement, *The 12th International Conference on Machine Vision*, 2019 (Accepted).
- [44] W. Wang, X. Yuan, X. Wu, et al., Dehazing for images with large sky region, *Neurocomputing* 238 (5) (2017) 365–376 2017.
- [45] W. Wang, X. Yuan, X. Wu, et al., Fast Image dehazing method based on linear transformation, *IEEE Trans. Multimedia* 19 (6) (2017) 1142–1155.
- [46] Y. Wang, Q. Chen, B. Zhang, Image enhancement based on equal area dualistic sub-image histogram equalization method, *IEEE Trans. Consum. Electron.* 45 (1) (1999) 68–75.
- [47] Z. Ying, G. Li, Y. Ren, et al., A new image contrast enhancement algorithm using exposure fusion framework, in: *International Conference on Computer Analysis of Images and Patterns*, 2017, pp. 36–46.
- [48] C. Yu, Y. Ouyang, C. Wang, et al., Adaptive inverse hyperbolic tangent algorithm for dynamic contrast adjustment in displaying scenes, *EURASIP J. Advan. Signal Process.* 1 (2010) 1–20.
- [49] L. Zhang, P. Shen, X. Peng, et al., Simultaneous enhancement and noise reduction of a single low-light image, *IET Image Proc.* 10 (11) (2017) 840–847.
- [50] N. Zhi, S. Mao, M. Li, Enhancement algorithm based on illumination adjustment for non-uniform illuminance video images in coal mine, *Meitan Xuebao/J. China Coal Soc.* 42 (8) (2017) 2190–2197.